Bacteriophage cooperation suppresses CRISPR-Cas3 and Cas9 immunity

Adair L. Borges[1], Jenny Y. Zhang[1], MaryClare F. Rollins[2], Beatriz A. Osuna[1], Blake Wiedenheft[2], Joseph Bondy-Denomy[1,3*]

[1]Department of Microbiology and Immunology, University of California San Francisco, San Francisco, CA 94143, USA
[2] Department of Microbiology and Immunology, Montana State University, Bozeman, MT 59717, USA.
[3]Quantitative Biosciences Institute, University of California San Francisco, San Francisco, CA 94143, USA

*Correspondence: joseph.bondy-denomy@ucsf.edu

SUMMARY

Bacteria utilize CRISPR-Cas adaptive immune systems for protection from bacteriophages (phages), and some phages produce anti-CRISPR (Acr) proteins that inhibit immune function. Despite thorough mechanistic and structural information for some Acr proteins, how they are deployed and utilized by a phage during infection is unknown. Here, we show that Acr production does not guarantee phage replication, but instead, infections fail when phage population numbers fall below a critical threshold. Failing infections can be rescued by related phages that act as Acr donors, demonstrating that infections succeed if a sufficient Acr dose is contributed to a single cell by multiple phage genomes. The production of Acr proteins by phage genomes that fail to replicate leave the cell immunosuppressed, which predisposes the cell for successful infection by other phages in the population. This "cooperative" phage mechanism for CRISPR-Cas inhibition demonstrates inter-virus cooperation that may also manifest in other host-parasite interactions.

INTRODUCTION

Bacteria and the viruses that infect them (phages) are engaged in an ancient evolutionary arms race, which has resulted in the emergence of a diversity of CRISPR-Cas (clustered regularly interspaced short palindromic repeats and CRISPR-associated genes) adaptive immune systems (Koonin et al., 2017). CRISPR-Cas immunity is powered by the acquisition of small fragments of phage genomes into the bacterial CRISPR array, the subsequent transcription and processing of these arrays to generate small CRISPR RNAs, and the RNA-guided destruction of the phage genome (Barrangou et al., 2007; Brouns et al., 2008; Garneau et al., 2010; Levy et al., 2015). The destruction of foreign DNA by CRISPR-Cas has been shown to prevent the acquisition of plasmids, DNA from the environment, phage lytic replication, and prophage integration (Barrangou et al., 2007; Bikard et al., 2012; Cady et al., 2012; Edgar and Qimron, 2010; Garneau et al., 2010). In bacterial populations, these systems provide a fitness advantage to their host microbe during times of phage presence in the environment (van Houte et al., 2016; Westra et al., 2015).

To combat the potent action of RNA-guided CRISPR-Cas nucleases, phages have developed inhibitor proteins called anti-CRISPRs (Acrs). Acr proteins have been

discovered in phages, prophages, mobile islands, and core genomes across many distinct bacteria and archaea (Borges et al., 2017; He et al., 2018; Pawluk et al., 2017). Specific Acr proteins inhibit the Type I-F, I-E, and I-D CRISPR-Cas3 have been identified (Bondy-Denomy et al., 2013; He et al., 2018; Pawluk et al., 2014; 2016b), and also other Acr proteins that inhibit Type II-A and II-C (Hynes et al., 2017; Pawluk et al., 2016a; Rauch et al., 2017) CRISPR-Cas9 systems. Phylogenetic studies indicate that these proteins are likely ubiquitous in coevolving populations of bacteria and phages (Pawluk et al., 2017) and provide a significant replicative advantage to phages in the presence of CRISPR immunity (van Houte et al., 2016).

Anti-CRISPRs were first identified in phages that neutralize the *Pseudomonas aeruginosa* type I-F system (anti-CRISPR type I-F, AcrIF1-5)(Bondy-Denomy et al., 2013), and five more I-F anti-CRISPRs (AcrIF6-10) were subsequently identified in various mobile genetic elements (Pawluk et al., 2016b). The I-F Csy surveillance complex (also called I-F Cascade) is comprised of four proteins (Csy1-4) and a *trans*-acting nuclease/helicase protein, Cas2/3 (Rollins et al., 2017; Wiedenheft et al., 2011). Anti-CRISPR proteins function by interacting directly with the Csy complex and inhibit DNA binding or bind to Cas2/3 and prevent nuclease-mediated degradation (Bondy-Denomy et al., 2015). The structures of type I-F Acr proteins AcrIF1, AcrIF2, and AcrIF3 have been solved in complex with their target proteins, revealing mechanistically distinct inhibitors that bind tightly to their target Cas protein (Chowdhury et al., 2017; Guo et al., 2017; Maxwell et al., 2016; Wang et al., 2016). Together with the recent identification and characterization of proteins that inhibit Cas9, a common theme in Acr function has been revealed; all characterized Acr proteins block phage DNA binding or cleavage (Dong et al., 2017; Harrington et al., 2017; Pawluk et al., 2016a; Rauch et al., 2017).

Despite a detailed mechanistic understanding, however, it is unknown how anti-CRISPR proteins protect a phage during infection. Where phage DNA cleavage has been assessed *in vivo*, it occurs in as little as 2 minutes (Garneau et al., 2010), suggesting that CRISPR attack may outpace the ability of *de novo* Acr synthesis and action. During phage infection, we hypothesized that successful inhibition of CRISPR-Cas immunity by Acr proteins would be challenging, as all components of the *P. aeruginosa* immune system are expressed prior to phage infection (Bondy-Denomy et al., 2013; Cady et al., 2012).

83

84 Here, we utilize the diverse array of AcrIF proteins encoded by phages to demonstrate
85 that CRISPR-Cas inactivation is a challenge, and that the sufficient concentration of Acr
86 proteins necessary to inactivate CRISPR-Cas is contributed by multiple phage genomes.
87 While initial phage infections may fail, due to the rapid action of the CRISPR-Cas
88 system, immunosuppression can result due to the production of Acr proteins, which
89 leads to a population-level benefit for other phages. We propose that pathogens can
90 contribute to the "remodeling" of their host cell via rapid protein production, even if the
91 initial infecting genomes are cleared, opening the door for their clones .

92

93 **RESULTS**

94 **Anti-CRISPR proteins are imperfect CRISPR-Cas inhibitors**

95 We utilized the diversity of *acr* genes encoded by phages infecting *P. aeruginosa* to
96 determine the mechanism of CRISPR-Cas neutralization during infection. Five natural
97 phages, each encoding a single *acrIF* gene, were selected to represent *acrIF1-IF4* and
98 *acrIF7* (*acrIF5* does not exist as the sole *acrIF* gene on any phage, *acrIF6, F8-F10* are
99 not encoded by this phage family). Three of the five phages exhibited reduced efficiency
100 of plaquing (EOP) on *P. aeruginosa* strain PA14, possessing a type I-F CRISPR-Cas
101 system (Figure 1A, WT:pEmpty normalized to plaquing on ΔCRISPR). Overexpression of
102 a targeting crRNA (WT:pSp1) exacerbated anti-CRISPR inefficiency, limiting the
103 replication of all anti-CRISPR phages by at least one order of magnitude. This suggests
104 that anti-CRISPR proteins are unable to fully protect their associated phage genome.

105

106 To assess anti-CRISPR strength directly, an isogenic phage panel was generated by
107 replacing the *acrIE3* gene of phage DMS3m with single *acrIF* genes *F1-F7* ($DMS3m_{acrIF1}$-
108 $DMS3m_{acrIF7}$, Figure S1). WT PA14 (1 spacer targeting DMS3m, "1sp") and a laboratory
109 evolved strain (5 spacers targeting DMS3m, "5sp") were challenged with the
110 recombinant phages, revealing that all anti-CRISPRs are imperfect during infection
111 (Figure 1B). For phages encoding *acrIF1, F2, F3, F6* or *F7*, >90% of phage in the
112 population failed to replicate (EOP=10^{-1}) when faced with 5 targeting spacers. *acrIF4*
113 and *F5* were very weak, with 99.0-99.99% of phages failing to replicate, depending on
114 the CRISPR spacer content. We conclude that phages encoding *acrs* remain sensitive to
115 CRISPR-Cas immunity, suggesting that anti-CRISPR deployment and action is an
116 imperfect process.

117

118 The observation above identified groups of “strong” and “weak” Acr proteins. We
119 selected one representative from each group, and a third Acr that does not target the I-F
120 CRISPR system (i.e. AcrIE3), as a negative control. AcrIF1 was selected as a model
121 strong inhibitor, as its mechanism and binding affinity are known (Csy complex binding,
122 K_D = 2.5 x 10^{-11} M (Bondy-Denomy et al., 2015; Chowdhury et al., 2017)). In contrast,
123 AcrIF4 is a weak inhibitor that also binds the Csy complex (Bondy-Denomy et al., 2015),
124 but with a significantly slower on-rate and faster off-rate compared to AcrIF1 (Figure 1C,
125 Figure S2).

126

127 We next assessed the survival of bacterial cell populations over time, when infected with
128 phages that must deploy Acr proteins, but where apparently only a minority of the
129 population actually replicates. Phages were locked in the lytic cycle for the purpose of
130 this experiment, by knocking out the *C repressor* gene (*gp1*) in DMS3m$_{acrIF1}$,
131 DMS3m$_{acrIF4}$, and DMS3m$_{acrIE3}$, to enable the tracking of bacterial survival over time. The
132 virulent (vir) phages were used to infect 5sp strains in liquid culture, and bacterial growth
133 measured. Given the >4 order of magnitude difference in the KD of AcrIF1 and AcrIF4
134 for their binding partner, we reasoned that different phage concentrations may be
135 required to inactivate CRISPR-Cas function. In the presence of CRISPR immunity,
136 bacterial death only occurred at multiplicities of infection (MOI, input plaque forming units
137 per colony forming unit) greater than 0.02 for the strong *acrIF1* (Figure 2A) and greater
138 than an MOI of 2.0 (≥10^7 PFU) for the weak *acrIF4* (Figure 2B). Despite this high MOI-
139 dependence, no selection or evolution of phage DMS3m$_{acrIF4}$ occurred throughout the
140 experiment, as output phages remained as sensitive to CRISPR-Cas immunity as the
141 input population (Figure S3). The phage encoding *acrIE3* had no impact on bacterial
142 survival when faced with CRISPR immunity (Figure 2C), while in the absence of
143 CRISPR, phages at all concentrations cleared bacterial cultures (Figure 2D-2F). These
144 data demonstrate for bacterial lysis to occur, a critical phage concentration threshold
145 exists that is inversely proportional to Acr strength.

146

147 **Lytic replication requires a critical Acr protein concentration**

148 Concentration-dependent success of CRISPR-Cas neutralization during phage infection
149 could be caused by an excess of phage DNA targets that overwhelm a cell by titrating
150 away the Csy complexes, or by the contribution of Acr proteins from multiple phage

151 genomes in a single cell. To experimentally address these models, we genetically
152 modified phages to render them non-replicative, thus allowing the independent titration
153 of a subset of phages in the population. The C repressor gene (gp1) and surrounding
154 immunity region from phage JBD30 was introduced into DMS3m phages, generating a
155 hybrid phage (Figure S4A), whose replication could be prevented by the overexpression
156 of the JBD30 C repressor (*gp1*, Figure S4B). The JBD30 C repressor does not impact
157 the replication of DMS3 phages, however, as they are from different immune families
158 (heteroimmunity). In the presence of the JBD30 C repressor, high doses of the hybrid
159 phage did not replicate, confirming the efficacy of *gp1* overexpression (Figure S4C). This
160 enabled the mixing of two independent phage populations, where the replication of one
161 could be experimentally blocked, rendering it a sacrificial genome and Acr "donor". This
162 was used to assess the Acr concentration dependency model.
163
164 In the presence of sacrificial donor phages encoding AcrIF1, we observed a striking
165 contribution to CRISPR-Cas neutralization. This enabled DMS3m$_{acrIF1}$ (Figure 2G) and
166 DMS3m$_{acrIF4}$ (Figure 2H) to replicate from input MOIs that are unsuccessful in the
167 absence of the donor phage (Figure 2H,2G see "buffer"). Although the input
168 concentration of donor phages was modest (10^6 PFU, MOI = 0.2), this enabled the
169 replicative phage to achieve an increase of titers by 4-5 orders of magnitude. However,
170 this helping effect was not observed when the replicative phage did not encode an AcrIF
171 protein (Figure 2I), or when the donor phage produced *acrIE3* (Figure 2H-2I).
172 Additionally, any potential lysogens formed by the DMS3m donor phage in this
173 experiment would not have amplified the replicating phage, as these lysogens remain
174 resistant to superinfection (Figure S4D)**.** These data demonstrate that Csy complex
175 titration by infecting phage genomes alone does not appear to be a significant "anti-
176 CRISPR" factor in the outcome of phage replication or bacterial survival. Instead, the
177 determinant of phage replicative success is the concentration of Acr proteins reached in
178 single cells, which is achievable by Acr production from independent phage genomes.
179 This suggests that multiple phage genomes can contribute to the "immunosuppression"
180 of a single host by contributing separate doses of Acr protein, potentially explaining the
181 observed concentration thresholds and inefficiencies observed in plaquing
182 measurements.
183
184 **Lysogeny requires Acr proteins contributed by transient intracellular genomes**

185 All phages encoding Acr proteins that infect *P. aeruginosa* are naturally temperate, and
186 can form lysogens by integrating into the bacterial genome. We therefore measured the
187 impact of CRISPR and Acr proteins on lysogeny establishment during a single round of
188 infection. While previous experiments examined cumulative phage replication in the lytic
189 cycle over many hours, assaying lysogen formation over a short time frame is ideal for
190 understanding the initial events that determine phage genome survival or cleavage.
191 Additionally, lysogeny provides a direct readout for phage genome survival (i.e. an
192 integrated prophage), while in lytic replication, phage survival leads to a dead cell that
193 cannot be recovered. For these experiments, we selected the weak AcrIF4 protein as it
194 provided the largest dynamic range of inefficiency in a single round of infection.
195
196 We generated derivatives of DMS3m$_{acrIF4}$ and DMS3m$_{acrIE3}$ marked with a gentamicin
197 resistance cassette at the end of the genome, replacing a nonessential gene, *gp52*. This
198 allowed the independent titration of two distinct replication-competent phage populations
199 and the selection and analysis of stable lysogens after the experiment. These phages
200 were used to infect ΔCRISPR cells (0sp) for a time span less than a single round of
201 infection (50 minutes, Figure S5), and the number of gentamicin resistant lysogens was
202 assessed. In the absence of CRISPR selection, a linear increase in the number of
203 lysogens with increasing MOI was observed, over ~4 orders of magnitude (Figure 3A-
204 3B, circles). In the presence of spacers targeting DMS3m (5sp), CRISPR reduced the
205 efficiency of lysogeny (EOL, compared to 0sp) for the weak *acr* phage DMS3m$_{acrIF4}$, to
206 such a degree that lysogeny was undetectable at low MOIs, and impaired by 100-1000-
207 fold at higher MOIs (Figure 3A, triangles). DMS3m$_{acrIF4}$ demonstrated concentration
208 dependence for successful lysogeny, with EOL values below or at the limit of detection
209 for lower MOIs, increasing to EOL = 0.01 at higher MOIs (Figure 3C). Phage
210 DMS3m$_{acrIE3}$ formed no lysogens at all input concentrations tested, demonstrating that
211 Acr-mediated immune suppression is required to establish lysogeny (Figure 3B, 3D).
212
213 We hypothesized that Acr concentration dependence for CRISPR neutralization during
214 lysogeny could also be explained by phage cooperation, and that below threshold
215 concentrations of DMS3m$_{acrIF4}$ could be rescued by the addition of Acr donor phages *in*
216 *trans*. To test this hypothesis, we infected the 5sp strain with a mixture of 10^3 LFU
217 DMS3m$_{acrIF4}$ *gp52::gent* and 10^7 PFU of unmarked Acr donor phages, and measured the
218 EOL of DMS3m$_{acrIF4}$ *gp52::gent*. The EOL of DMS3m$_{acrIF4}$ *gp52::gent* increased by 2

219 orders of magnitude with Acr donor phage DMS3m$_{acrIF1}$, while DMS3m$_{acrIF4}$ donor phage
220 increased EOL by 1 order of magnitude (Figure 3E). No such increase in lysogeny was
221 observed for a phage without an *acrIF* gene, DMS3m$_{acrIE3}$ *gp52::gent* (Figure 3F). The
222 addition of Acr donor phages DMS3m$_{acrIE3}$, or an escaper phage DMS3m$_{acrIE3}$* had no
223 effect on the EOL of the marked DMS3m$_{acrIF4}$ phage, demonstrating that the donor
224 phage must be an Acr-producer.
225
226 To determine the specific mechanism of anti-CRISPR donation leading to survival
227 DMS3m$_{acrIF4}$ *gp52::gent*, we used the resulting lysogens as a genetic record of infection
228 success for both the marked phage and the unmarked phage. This family of Mu-like
229 phages integrates randomly into the host genome, and therefore strains with multiple
230 prophages are possible (Bondy-Denomy et al., 2016). We assayed the lysogens
231 resulting from the experiment described above for the presence of the donor phage
232 genome in addition to the DMS3m$_{acrIF4}$ *gp52::gent* prophage. All resulting lysogens tested
233 (n=48) possessed only the marked prophage, with none possessing the Acr donor
234 prophage (Figure S6). This demonstrates that the transient presence of the Acr donor
235 phage genome (i.e. no lysogeny) in the same cell was sufficient to generate enough Acr
236 protein to protect the marked phage, leading to the establishment of lysogens that would
237 not exist if not for the Acr donor (Figure 3E, compare "buffer" to "IF1"). The only time rare
238 double lysogens were isolated, was when the marked phage DMS3m$_{acrIE3}$ *gp52::gent*
239 was used with the unmarked DMS3m$_{acrIF1}$ Acr donor phage (Figure 3F), since the
240 prophage encoding *acrIE3* would be unable to neutralize CRISPR-Cas after lysogenic
241 establishment and long-lasting protection from the donor prophage was required.
242 Collectively, these data are consistent with a model where the production of Acr proteins
243 from a transient phage genome prior to its cleavage generates an immunosuppressed
244 cell that can be successfully parasitized by another phage upon re- or co-infection(s).
245
246 **Stoichiometric inhibitors of Cas9 required bacteriophage cooperation**
247 The intrinsic inefficiency of stoichiometric inhibitors is likely due to the requirement for
248 the rapid synthesis of a high concentration of inhibitors before phage genome cleavage.
249 To determine whether this model generally applies to other stoichiometric inhibitors of
250 bacterial immunity, we engineered a *P. aeruginosa* strain to express the Cas9 protein
251 from *Streptococcus pyogenes* (SpyCas9) and a DMS3m phage to express a previously
252 identified Cas9 inhibitor, AcrIIA4 (Dong et al., 2017; Rauch et al., 2017). With this

253 entirely heterologous system, we again observed inefficiency for a phage relying on an
254 Acr protein. Spot-titration of phage lysates on a strain expressing a single guide RNA
255 (sgRNA) targeting DMS3m decreased the titer of DMS3m$_{acrIE3}$ by many orders of
256 magnitude, while DMS3m$_{acrIIA4}$ was protected (Figure 4A). However, quantification of the
257 efficiency of plaquing again revealed that relying on an Acr protein for replication is
258 imperfect, with an EOP = 0.4 (Figure 4B). In lytic replication infection experiments,
259 DMS3m$_{acrIIA4}$ displayed concentration-dependent bacterial lysis in the presence of
260 CRISPR targeting (Figure 4C), while infection with DMS3m$_{acrIE3}$ did not affect bacterial
261 growth (Figure 4D). In the absence of CRISPR-Cas targeting, however, both phages
262 killed their hosts at all phage concentrations tested (Figure 4E, 4F). To determine
263 whether this concentration dependence for Cas9 inhibition was also a result of
264 insufficient intracellular Acr dose, a non-replicative hybrid DMS3m$_{AcrIIA4}$ phage was
265 generated and used as a donor during infection. Indeed, increased delivery of AcrIIA4 to
266 cells allowed DMS3m$_{acrIIA4}$ to replicated robustly from a concentration that was previously
267 unsuccessful (Figure 4G), demonstrating phage cooperation to neutralize CRISPR-
268 Cas9. Unlike CRISPR-Cas3 experiments described previously, where 5 spacers were
269 targeted to the DMS3m phage, here a single spacer sequence was used, which allowed
270 for phage escape mutations to occur. Because of this, we observed that DMS3m$_{acrIE3}$
271 could also be helped by increased doses of AcrIIA4 from the phage population (Figure
272 4H), likely protecting the genome *in trans*, enabling escaper evolution.
273
274 **DISCUSSION**
275 Here we demonstrate that the necessary intracellular concentration of an anti-immunity
276 protein to achieve inactivation of cellular immunity depends on the relative strengths of
277 both the inhibitor and the immunity pathway, which dictates the number of infecting
278 viruses required in the population. We conclude that a single cell can become
279 immunosuppressed by anti-immune protein contributions from independent infection
280 events. In the absence of viral replication, these infection events serve to contribute to
281 the inactivation of cellular immunity, thus enhancing the probability of successful
282 infection events in the future (Figure 5). We expect that cooperation of this sort is
283 necessary when the immune process acts rapidly and irreversibly on the infecting viral
284 genome, as CRISPR-Cas immunity does.
285

286 The ability of phages to replicate in the lytic cycle or establish lysogens is impacted
287 dramatically by the number of phages in the population. To demonstrate phage-phage
288 cooperation for the deployment of Acr proteins, three distinct genetic strategies were
289 used, allowing the independent titration of phages encoding a defined Acr protein: i) non-
290 replicative Acr donor phages, ii) marked and unmarked phages to follow the fate of only
291 one phage, and iii) the prophage status of lysogens, as a genetic record of phage
292 success. By restricting the replication of a subset of phages, we could track the lytic
293 replication of a low-dose of wild-type phages in the presence of DNA target or Acr
294 donors to determine the molecular determinants of density-dependent phage replication.
295 In contrast, the prophage acquisition experiment allows a more natural scenario, where
296 all phages are capable of replication, but an antibiotic resistance marker allows us to
297 track the outcome of one phage genotype, starting from a concentration below its
298 threshold for successful lysogeny. This demonstrated that wild-type Acr-donor phages in
299 the population contribute to cellular immunosuppression, enabling the formation of
300 lysogens that did not occur in their absence. The presence of only a single, marked
301 prophage in the bacterial genome proves that the donor phage neither entered the lytic
302 cycle (this would kill the cell), nor lysogenized (prophage would be present), but had
303 been present in the cell transiently.
304
305 The key result here is the observation that phages can remodel their host cell, even in
306 the absence of a replicating or integrated genome. It has long been known that
307 integrated prophages modulate host phenotypes via gene expression, including
308 superinfection exclusion, toxin production, and the production of Acr proteins (Bondy-
309 Denomy et al., 2013; Bondy-Denomy and Davidson, 2014; Bondy-Denomy et al., 2016;
310 Waldor and Mekalanos, 1996; Weigle and Delbruck, 1951). Although less commonly
311 described, there is also precedent for lytic phages to impact an interaction with other
312 phages during replication. The Imm protein produced by the phage T4 prevents other
313 phages in the environment from infecting the cell that one phage is currently replicating
314 within (Lu and Henning, 1989). This has been attributed to preventing superinfection and
315 the potential disruption of the carefully timed phage replication cycle. This supports a
316 conclusion that co- and/or re-infections are a common occurrence in nature. However,
317 here, we propose a new model of phage-induced host remodeling, whereby a transient-
318 unsuccessful infection produces proteins that inactivate defense, enabling future

infections. This altruism would be evolutionarily advantageous to phage clones within the population, where all are providing Acr proteins to neutralize CRISPR.

A distinct, but notable observation from this work is that not all Acr proteins operate at equivalent strengths. However, encoding even a weak inhibitor (e.g. AcrIF4). still provides a significant advantage to the phage, compared to lacking them entirely. We show that AcrIF4 binds the Csy complex with affinities that are orders of magnitude weaker than Acr proteins like AcrIF1. We selected AcrIF1 as a model strong Acr protein because of its comparable mechanism of action to AcrIF4 (i.e. Csy complex binding), and consider it representative of other strong Acr proteins (AcrIF2, F3, F6, F7), based on EOP data. Going forward, we speculate that the strongest Acr proteins would be enzymatic in nature, allowing rapid and efficient inactivation of CRISPR complexes in a sub-stoichiometric manner, although no such Acr mechanism has been discovered. While not an enzyme, the recent demonstration of the AcrIIC3 protein inactivating two Cas9 proteins at the same time would likely be a more efficient path towards CRISPR neutralization (Harrington et al., 2017).

The challenge of neutralizing a pre-expressed CRISPR-Cas system likely explains why stoichiometric inhibitors like Acr proteins are imperfect, and phages relying on them are partially targeted by CRISPR. The sacrificial, population-level aspect of CRISPR inhibition is reminiscent of the manifestations of CRISPR adaptation in populations of bacterial cells. The majority of infected naïve host cells die, before a clone with a new spacer emerges (Barrangou et al., 2007; Hynes et al., 2014). In the case of anti-immunity, many phages die in order to inhibit CRISPR on a single cell level, and this must happen at sufficient frequency within an ecosystem for phage to prevail. We suspect that this mechanism of cellular immunosuppression and inter-parasite cooperation may have parallels in other host-pathogen interactions, where concentration dependence manifests at predictable levels due the strengths of immune and anti-immune processes.

SUPPLEMENTAL INFORMATION

Figures S1-S6 are provided separately.

AUTHOR CONTRIBUTIONS

A.L.B. and J.B.D. designed experiments and wrote the manuscript. A.L.B. engineered phage variants and conducted all experiments with the exception of binding affinity measurements. J.Y.Z. assisted with experimental design and execution, phage engineering, and data collection. B.A.O. built the Cas9 strain in *Pseudomonas aeruginosa.* J.B.D. supervised experiments. M.R. conducted Acr binding affinity measurements under the supervision of B.W. All authors contributed to data analysis and edited the manuscript.

ACKNOWLEDGEMENTS

The Bondy-Denomy lab was supported by the University of California San Francisco Program for Breakthrough in Biomedical Research, funded in part by the Sandler Foundation, and an NIH Office of the Director Early Independence Award (DP5-OD021344). Research in the Wiedenheft lab is supported by the National Institutes of Health (P20GM103500, P30GM110732, R01GM110270, R01GM108888 and R21 AI130670), the National Science Foundation EPSCoR (EPS-110134), the M. J. Murdock Charitable Trust, a young investigator award from Amgen, and the Montana State University Agricultural Experimental Station (USDA NIFA). The laboratory evolved PA14 strain with 5 spacers targeting DMS3 was generously provided by Stineke van Houte and Edze Westra (University of Exeter).

373 **REFERENCES**

374 Barrangou, R., Fremaux, C., Deveau, H., Richards, M., Boyaval, P., Moineau, S.,
375 Romero, D.A., and Horvath, P. (2007). CRISPR provides acquired resistance against
376 viruses in prokaryotes. Science *315*, 1709–1712.

377 Bikard, D., Hatoum-Aslan, A., Mucida, D., and Marraffini, L.A. (2012). CRISPR
378 interference can prevent natural transformation and virulence acquisition during in vivo
379 bacterial infection. Cell Host Microbe *12*, 177–186.

380 Bondy-Denomy, J., Pawluk, A., Maxwell, K.L., and Davidson, A.R. (2013).
381 Bacteriophage genes that inactivate the CRISPR/Cas bacterial immune system. Nature
382 *493*, 429–432.

383 Bondy-Denomy, J., and Davidson, A.R. (2014). When a virus is not a parasite: the
384 beneficial effects of prophages on bacterial fitness. J Microbiol *52*, 235–242.

385 Bondy-Denomy, J., Garcia, B., Strum, S., Du, M., Rollins, M.F., Hidalgo-Reyes, Y.,
386 Wiedenheft, B., Maxwell, K.L., and Davidson, A.R. (2015). Multiple mechanisms for
387 CRISPR-Cas inhibition by anti-CRISPR proteins. Nature *526*, 136–139.

388 Bondy-Denomy, J., Qian, J., Westra, E.R., Buckling, A., Guttman, D.S., Davidson, A.R.,
389 and Maxwell, K.L. (2016). Prophages mediate defense against phage infection through
390 diverse mechanisms. The ISME Journal *10*, 2854–2866.

391 Borges, A.L., Davidson, A.R., and Bondy-Denomy, J. (2017). The Discovery,
392 Mechanisms, and Evolutionary Impact of Anti-CRISPRs. Annual Review of Virology *4*,
393 annurev–virology–101416–041616.

394 Brouns, S.J.J., Jore, M.M., Lundgren, M., Westra, E.R., Slijkhuis, R.J.H., Snijders,
395 A.P.L., Dickman, M.J., Makarova, K.S., Koonin, E.V., and van der Oost, J. (2008). Small
396 CRISPR RNAs guide antiviral defense in prokaryotes. Science *321*, 960–964.

397 Cady, K.C., Bondy-Denomy, J., Heussler, G.E., Davidson, A.R., and O'Toole, G.A.
398 (2012). The CRISPR/Cas adaptive immune system of Pseudomonas aeruginosa
399 mediates resistance to naturally occurring and engineered phages. *194*, 5728–5738.

400 Chowdhury, S., Carter, J., Rollins, M.F., Golden, S.M., Jackson, R.N., Hoffmann, C.,
401 Nosaka, L., Bondy-Denomy, J., Maxwell, K.L., Davidson, A.R., et al. (2017). Structure
402 Reveals Mechanisms of Viral Suppressors that Intercept a CRISPR RNA-Guided
403 Surveillance Complex. Cell *169*, 47–57.e11.

404 Dong, D., Guo, M., Wang, S., Zhu, Y., Wang, S., Xiong, Z., Yang, J., Xu, Z., and Huang,
405 Z. (2017). Structural basis of CRISPR-SpyCas9 inhibition by an anti-CRISPR protein.
406 Nature.

407 Edgar, R., and Qimron, U. (2010). The Escherichia coli CRISPR system protects from λ
408 lysogenization, lysogens, and prophage induction. J. Bacteriol. *192*, 6291–6294.

409 Garneau, J.E., Dupuis, M.-È., Villion, M., Romero, D.A., Barrangou, R., Boyaval, P.,
410 Fremaux, C., Horvath, P., Magadán, A.H., and Moineau, S. (2010). The CRISPR/Cas
411 bacterial immune system cleaves bacteriophage and plasmid DNA. Nature *468*, 67–71.

412 Guo, T.W., Bartesaghi, A., Yang, H., Falconieri, V., Rao, P., Merk, A., Eng, E.T.,
413 Raczkowski, A.M., Fox, T., Earl, L.A., et al. (2017). Cryo-EM Structures Reveal
414 Mechanism and Inhibition of DNA Targeting by a CRISPR-Cas Surveillance Complex.
415 Cell *171*, 414–426.e12.

416 Harrington, L.B., Doxzen, K.W., Ma, E., Liu, J.-J., Knott, G.J., Edraki, A., Garcia, B.,
417 Amrani, N., Chen, J.S., Cofsky, J.C., et al. (2017). A Broad-Spectrum Inhibitor of
418 CRISPR-Cas9. Cell.

419 He, F., Bhoobalan-Chitty, Y., Van, L.B., Kjeldsen, A.L., Dedola, M., Makarova, K.S.,
420 Koonin, E.V., Brodersen, D.E., and Peng, X. (2018). Anti-CRISPR proteins encoded by
421 archaeal lytic viruses inhibit subtype I-D immunity. Nature Microbiology 1.

422 Hynes, A.P., Rousseau, G.M., Lemay, M.-L., Horvath, P., Romero, D.A., Fremaux, C.,
423 and Moineau, S. (2017). An anti-CRISPR from a virulent streptococcal phage inhibits
424 Streptococcus pyogenes Cas9. Nature Microbiology *315*, 1.

425 Hynes, A.P., Villion, M., and Moineau, S. (2014). Adaptation in bacterial CRISPR-Cas
426 immunity can be driven by defective phages. Nature Communications *5*, 4399.

427 Koonin, E.V., Makarova, K.S., and Wolf, Y.I. (2017). Evolutionary Genomics of Defense
428 Systems in Archaea and Bacteria. Annu Rev Microbiol *71*, annurev–micro–090816–
429 093830.

430 Levy, A., Goren, M.G., Yosef, I., Auster, O., Manor, M., Amitai, G., Edgar, R., Qimron,
431 U., and Sorek, R. (2015). CRISPR adaptation biases explain preference for acquisition
432 of foreign DNA. *520*, 505–510.

433 Lu, M.J., and Henning, U. (1989). The immunity (imm) gene of Escherichia coli
434 bacteriophage T4. Journal of Virology *63*, 3472–3478.

435 Maxwell, K.L., Garcia, B., Bondy-Denomy, J., Bona, D., Hidalgo-Reyes, Y., and
436 Davidson, A.R. (2016). The solution structure of an anti-CRISPR protein. Nature
437 Communications *7*, 13134.

438 Pawluk, A., Amrani, N., Zhang, Y., Garcia, B., Hidalgo-Reyes, Y., Lee, J., Edraki, A.,
439 Shah, M., Sontheimer, E.J., Maxwell, K.L., et al. (2016a). Naturally Occurring Off-
440 Switches for CRISPR-Cas9. Cell *167*, 1829–1838.e1829.

441 Pawluk, A., Bondy-Denomy, J., Cheung, V.H.W., Maxwell, K.L., and Davidson, A.R.
442 (2014). A new group of phage anti-CRISPR genes inhibits the type I-E CRISPR-Cas
443 system of Pseudomonas aeruginosa. mBio *5*, e00896–e00896–14.

444 Pawluk, A., Davidson, A.R., and Maxwell, K.L. (2017). Anti-CRISPR: discovery,
445 mechanism and function. Nat Rev Micro *1*, nrmicro.2017.120.

446 Pawluk, A., Staals, R.H.J., Taylor, C., Watson, B.N.J., Saha, S., Fineran, P.C., Maxwell,
447 K.L., and Davidson, A.R. (2016b). Inactivation of CRISPR-Cas systems by anti-CRISPR
448 proteins in diverse bacterial species. Nature Microbiology *1*, 1–6.

449 Rauch, B.J., Silvis, M.R., Hultquist, J.F., Waters, C.S., McGregor, M.J., Krogan, N.J.,

450 and Bondy-Denomy, J. (2017). Inhibition of CRISPR-Cas9 with Bacteriophage Proteins.
451 Cell *168*, 150–158.e10.

452 Rollins, M.F., Chowdhury, S., Carter, J., Golden, S.M., Wilkinson, R.A., Bondy-Denomy,
453 J., Lander, G.C., and Wiedenheft, B. (2017). Cas1 and the Csy complex are opposing
454 regulators of Cas2/3 nuclease activity. Proceedings of the National Academy of
455 Sciences *23*, 201616395–E5121.

456 van Houte, S., Ekroth, A.K.E., Broniewski, J.M., Chabas, H., Ben Ashby, Bondy-
457 Denomy, J., Gandon, S., Boots, M., Paterson, S., Buckling, A., et al. (2016). The
458 diversity-generating benefits of a prokaryotic adaptive immune system. Nature *532*, 385–
459 388.

460 Waldor, M.K., and Mekalanos, J.J. (1996). Lysogenic conversion by a filamentous phage
461 encoding cholera toxin. Science *272*, 1910–1914.

462 Wang, X., Yao, D., Xu, J.-G., Li, A.-R., Xu, J., Fu, P., Zhou, Y., and Zhu, Y. (2016).
463 Structural basis of Cas3 inhibition by the bacteriophage protein AcrF3. Nat. Struct. Mol.
464 Biol. *23*, 868–870.

465 Weigle, J.J., and DELBRUCK, M. (1951). Mutual exclusion between an infecting phage
466 and a carried phage. J. Bacteriol. *62*, 301–318.

467 Westra, E.R., van Houte, S., Oyesiku-Blakemore, S., Makin, B., Broniewski, J.M., Best,
468 A., Bondy-Denomy, J., Davidson, A., Boots, M., and Buckling, A. (2015). Parasite
469 Exposure Drives Selective Evolution of Constitutive versus Inducible Defense. Curr. Biol.
470 *25*, 1043–1049.

471 Wiedenheft, B., van Duijn, E., Bultema, J.B., Bultema, J., Waghmare, S.P., Waghmare,
472 S., Zhou, K., Barendregt, A., Westphal, W., Heck, A.J.R., et al. (2011). RNA-guided
473 complex from a bacterial immune system enhances target recognition through seed
474 sequence interactions. Proceedings of the National Academy of Sciences *108*, 10092–
475 10097.

476

477 **FIGURE LEGENDS**

478 **Figure 1. Anti-CRISPRs are imperfect CRISPR-Cas inhibitors**

479 **(A)** Efficiency of plaquing (EOP) of 5 related phages bearing distinct *acrIF* genes
480 (JBD30$_{acrIF1}$, MP29$_{acrIF2}$, JBD88a$_{acrIF3}$, JBD24$_{acrIF4}$, LPB1$_{acrIF7}$) on *Pseudomonas*
481 *aeruginosa* strain PA14. Plaque forming units (PFUs) were quantified on wild-type PA14
482 with 1-2 natural targeting spacers (WT + pEmpty) or on PA14 overexpressing 1 targeting
483 spacer (WT + pSp1), then normalized to the number of PFUs measured on a non-
484 targeting PA14 derivative (0sp). Data are represented as the mean of 3 biological
485 replicates +/- SD.

486 **(B)** EOP of isogenic DMS3m phages with *acrIF1-7* or *acrIE3* in the DMS3m *acr* locus.
487 EOP was calculated as PFU counts measured on WT PA14 with 1 targeting spacer
488 (1sp) or a laboratory evolved PA14 derivative with 5 targeting spacers (5sp) normalized
489 to PFU counts measured on non-targeting PA14 (0sp). Data are represented as the
490 mean of 3 biological replicates +/- SD. ND, not detectable.
491 **(C)** Plot of association (Ka) and dissociation (Kd) rates for AcrIF1 (data adapted from
492 Chowdhury et al. 2017) and AcrIF4 binding the PA14 Csy complex. See Figure S2 for
493 SPR AcrIF4 sensogram.
494
495 **Figure 2. Anti-CRISPR success requires cooperative infections during lytic growth**
496 **(A-F)** 12 h growth curves of *P. aeruginosa* strain PA14 with 5 targeting spacers
497 (+CRISPR, panels **A-C**) or no CRISPR-Cas function (ΔCRISPR, **D-F**) infected with
498 virulent variants of DMS3m$_{acrIF1}$, DMS3m$_{acrIF4}$, or DMS3m$_{acrIE3}$ at multiplicity of infection
499 (MOI) increasing in 10-fold steps from $2x10^{-5}$ to $2x10^{1}$ (rainbow colors) or uninfected
500 (black). Colors correspond to the MOI legend and growth curves. OD600 is represented
501 as the mean of 3 biological replicates +/- SD. ND, not detectable.
502 **(G-I)** Replication of virulent DMS3m$_{acr}$ phages (target phage) in the presence of 10^{6} PFU
503 (MOI 0.2) hybrid phage (donor) in PA14 with 5 targeting spacers expressing the JBD30
504 C-repressor. Phages were harvested after 24 hours of co-culture and DMS3m$_{acr}$ phage
505 PFUs were quantified on PA14 0sp expressing the JBD30 C repressor. Phage output is
506 represented as the mean of 3 biological replicates +/- SD. ND, not detectable.
507
508 **Figure 3. Immunosuppression facilitates acquisition of a marked prophage**
509 (**A,B**) Acquisition of marked DMS3m$_{acrIF4}$ or DMS3m$_{acrIE3}$ prophage by PA14 with 0
510 spacers (0 sp, circles) or 5 targeting spacers (5 sp, triangles). This experiment was
511 performed in biological triplicate, and individual replicate values are displayed. LoD, limit
512 of detection.
513 (**C,D**) Efficiency of lysogeny (EOL) of DMS3m$_{acrIF4\ gp52::gentR}$ and
514 DMS3m$_{acrIE3\ gp52::gentR}$ in the presence of CRISPR targeting. EOL was calculated by
515 dividing the output lysogens forming units (LFUs) from the strain with 5 targeting spacers
516 (5sp) to the number of LFUs in PA14 with 0 targeting spacers (0sp). Data are
517 represented as the mean of 3 biological replicates +/- SD. ND, not detectable.
518 (**E,F**) EOL of 10^{3} LFUs of DMS3m$_{acrIF4\ gp52::gentR}$ and DMS3m$_{acrIE3\ gp52::gentR}$ in the presence
519 of 10^{7} PFU of the indicated DMS3m$_{acr}$ phage. Data are represented as the mean of 3

520 biological replicates +/- SD. ND, not detectable. See Figure S6 for lysogen genetic
521 analysis.
522
523 **Figure 4. Cas9 anti-CRISPR AcrIIA4 requires cooperative infection to neutralize**
524 **Type II-A CRISPR immunity**
525 **(A)** 10-fold serial dilutions of DMS3m$_{acrIE3}$ or DMS3m$_{acrIIA4}$ plated on a lawn of
526 *Pseudomonas aeruginosa* strain PAO1 expressing *Streptococcus pyogenes* Type II-A
527 Cas9 (PAO1::SpyCas9) and single guide RNA (+ sgRNA) or non-targeting control (+
528 vector).
529 **(B)** Efficiency of plaquing of DMS3m$_{acrIIA4}$ and DMS3m$_{acrIE3}$ was calculated by normalizing
530 PFU counts on a targeting strain of PAO1::SpyCas9 (+sgRNA) to PFU counts on a non-
531 targeting strain of PAO1::SpyCas9 (+vector). Data are represented as the mean of 3
532 biological replicates +/- SD. ND, not detectable.
533 **(C-F)** 12 hour growth curves of PAO1::spyCas9 expressing a targeting sgRNA (+
534 sgRNA, panels **C-D**) or a non-targeting vector control (+vector, E-F) that were infected
535 with virulent DMS3m$_{acrIIA4}$ or DMS3m$_{acrIE3}$ at multiplicities of infection (MOI, rainbow
536 colors) from $2x10^{-5}$ to $2x10^{-2}$. Growth curves of uninfected cells are shown in black.
537 OD600 values are represented as the mean of 3 biological replicates +/- SD.
538 **(G-H)** Replication of virulent DMS3m$_{acr}$ phages (target phage) in the presence of 10^7
539 PFU (MOI 2) hybrid phage (donor) in PAO1::SpyCas9 + sgRNA expressing the JBD30
540 C-repressor. Phages were harvested after 24 hours and DMS3m$_{acr}$ phage PFUs
541 quantified on PAO1::SpyCas9 + vector expressing the JBD30 C repressor. Phage output
542 is represented as the mean of 3 biological replicates +/- SD. ND, not detectable.
543
544 **Figure 5. Phage cooperation to suppress CRISPR-Cas immunity**
545 *Left*: Failed infections generate an immunosuppressed cell. While the phage genome
546 may be cleaved (dashed red line), Acr protein (small cyan circles) will be produced,
547 binding to some CRISPR-Cas complexes (larger purple structures, with crRNA). *Right:*
548 At low parasite density, it is unlikely the cell will be re-infected and the host will survive.
549 As high parasite density, the likelihood that the immunosuppressed cell with be re-
550 infected is higher. Co- or re-infection will lead to successful parasite replication and
551 amplification of the infectious population.
552
553 **SUPPLEMENTAL FIGURE LEGENDS**

554 **Figure S1. Engineering DMS3m$_{acr}$ phages**
555 **(A)** Schematic of two *acr* locus architectures used to generate an isogenic family of
556 DMS3m$_{acr}$ phages.
557 **(B)** Efficiency of plaquing (EOP) of DMS3m$_{acrIF1}$ with natural or synthetic locus
558 architecture on PA14 with 1 or 5 targeting spacers (1sp and 5 sp). Data are represented
559 as the mean of 3 biological replicates +/- SD.
560 **(C)** Table of DMS3m$_{acr}$ phage genotype and locus architecture, as well as the original
561 source of the *acr* gene and the corresponding accession number of the Acr protein.
562
563 **Figure S2. Sensograms of AcrIF4 and AcrIF1 binding the Csy complex**
564 **(A)** Sensogram showing real-time binding of increasing concentrations of free AcrIF4
565 (1.85 nM, 55.6 nM, 167 nM, 500 nM, 1.5 μM) to immobilized Csy complex. A model
566 describing Langmuir binding (black line) was fit to the data to calculate binding constants
567 (Ka, Kd, and KD; boxed inset).
568 **(B)** Sensogram showing real-time binding of increasing concentrations of free AcrIF1
569 (1.85 nM, 55.6nM, 167 nM, 500 nM, 1.5 μM) to immobilized Csy complex. A model
570 describing binding at a 2:1 stoichiometry of free analyte:immobilized ligand (black line)
571 was fit to the data to calculate binding constants (Ka1, Ka2,
572 Kd1, Kd2, and KD1, KD2; boxed inset) (Chowdhury and et al. 2017).
573
574 **Figure S3. Output phages from Figure 1B are CRISPR sensitive**
575 Efficiency of plaquing (EOP) of the original stock of virulent DMS3macr$_{IF4}$ (input) on
576 PA14 5 sp compared to EOP of DMS3m$_{acrIF4}$ harvested from high MOI infections (MOI 2,
577 MOI 20 output) from figure 2B. Data are represented as the mean of 3 biological
578 replicates +/- SD.
579
580 **Figure S4. Generating and validating Hybrid$_{acr}$ phages**
581 **(A)** 10-fold serial dilutions of DMS3m$_{acrIE3}$ and JBD30$_{acrIF1}$ spotted on lawns of non-
582 targeting (0sp) *Pseudomonas aeruginosa* PA14 expressing the DMS3m C repressor
583 (*gp1-DMS3m*), the JBD30 C repressor (*gp1-JBD30*) or a vector control.
584 **(B)** 10-fold serial dilutions of hybrid DMS3m$_{acrIE3\ gp1\text{-}JBD30}$ plated on lawns of non-targeting
585 (0sp) *Pseudomonas aeruginosa* PA14 expressing the DMS3m C repressor (*gp1-*
586 *DMS3m*), the JBD30 C repressor (*gp1-JBD30*), or a spacer which uniquely targets
587 JBD30 (2sp17).

588 **(C)** Hybrid phage (Hybrid$_{acrIF1}$ or Hybrid$_{acrIE3}$) harvested from infections of PA14 5sp
589 expressing the JBD30 C repressor from experiments shown in Figure 2G-I. Hybrid PFUs
590 were quantified on the 0sp PA14 strain. Data are represented as the mean of 3
591 biological replicates +/- SD.
592 **(D)** 10-fold serial dilutions of JBD30$_{acrIF1}$ or virulent DMS3m$_{acrIE3}$ spotted on lawns of
593 PA14 Δ*csy3* or PA14 Δ*csy3* lysogenized with Hybrid$_{acrIE3}$ or Hybrid$_{acrIF1}$. Despite being
594 heteroimmune with respect to DMS3, the DMS3 phage is unable to replicate well on this
595 lysogens due to other superinfection exclusion properties of DMS3.
596
597 **Figure S5. Timecourse of lysogen formation**
598 Time course of acquisition of gentamicin-resistance marked DMS3m$_{acrIFI\ gp52::gentR}$
599 prophage by a non-targeting (0 sp) strain of PA14, labeled with estimates of each
600 infectious cycle (Rounds 1-3). Data are represented as the mean of 3 biological
601 replicates +/- SD.
602
603 **Figure S6. Prophage content of lysogens from Figure 3E-F**
604 **(A)** 10-fold serial dilutions of supernatant harvested from overnight cultures of lysogens
605 from Figure 3E (1-48) and 3F (49-51), spotted on a non-targeting (0 sp) strain of PA14. A
606 faint clearing corresponds to induction of the gentamicin marked phage, while strong
607 plaquing (i.e. 50, 51) reflects the presence of the gentamicin marked phage and the
608 donor phage.
609 (**B**) PCR of genomic DNA harvested from harvested from overnight cultures of lysogens
610 from Figure 3E (1-48) and 3F (49-51) amplified with primers targeting *gp52-DMS3m* (top) or
611 the gentamicin resistance cassette used to replace *gp52* in *DMS3m*$_{acr\ gp52::gentR}$ derivatives
612 (bottom).
613
614 **METHODS**
615 **Strains and growth conditions**
616 *Pseudomonas aeruginosa* strains (UCBPP-PA14, PAO1) and *Escherichia coli* strains
617 were cultured on lysogeny broth (LB) agar or liquid media at 37C. LB was supplemented
618 with gentamicin (50 µg/mL for *P. aeruginos*a, 30 µg/mL for *E. coli*) to maintain the
619 pHERD30T plasmid or carbenicillin (250 µg/mL for *P. aeruginos*a, 100 µg/mL for *E. coli*)
620 to maintain pHERD20T or pMMBHE. To maintain pHERD30T and pMMBHE in the same
621 strain of *P. aeruginosa*, double selection of 30 µg/mL gentamicin and 100 µg/mL
622 carbenicillin was employed. In all *P. aeruginosa* experiments, expression from
623 pHERD20/30T was induced with 0.1%
624

625 **PAO1 SpyCas9 expression strain**
626 SpyCas9 expressed from the P_{LAC} promoter of pUC18T-mini-Tn7T-Gm was integrated
627 into the *P. aeruginosa* strain PAO1 chromosome by electroporation and Flp-mediated
628 marker excision as previously described (Choi and Schweizer, 2006). To generate the
629 heterologous Type II-A PAO1 strain the PAO1-attTn7::pUC18T-miniTn7T-P_{LAC}-SpyCas9
630 strain was transformed with pBAO72 (pMMB67HE-P_{LAC}-sgRNA) by electroporation. In all
631 experiments with this strain, SpyCas9 and the sgRNA were induced with 1mM IPTG.
632
633 **Construction of recombinant DMS3m$_{acr}$ phages**
634 DMS3m$_{acrIF1}$ was generated as in (Bondy-Denomy et al., 2013) by infecting cells
635 containing a recombination plasmid bearing JBD30 genes 34-38 (the anti-CRISPR locus
636 with large flanking regions). JBD30 naturally carries *acrIF1* and has high genetic
637 similarity to DMS3m$_{acrIE3}$, permitting for the selection of recombinant DMS3m phage
638 which had acquired *acrIF1*. To generate the extended panel of DMS3m$_{acr}$ phages in this
639 work, recombination cassettes were generated with regions from up and downstream the
640 anti-CRISPR genes from JBD30 Gibson assembled to flank the *acr* gene of interest on
641 pHERD20T or pHERD30T (see S1 for *acr* gene sources and exact details of *acr* locus
642 architecture). Recombinant phages were generated by infecting cells bearing these
643 recombination substrates. DMS3m$_{acr}$ phages were screened for their ability to resist
644 CRISPR targeting, and the insertion of the anti-CRISPR gene was confirmed by PCR.
645 Virulent derivatives of DMS3m$_{acr}$ phages were constructed by deleting gp1 (C repressor)
646 using materials and methods from Cady et al., 2012.
647
648 **Construction of DMS3m$_{acr\ gp52::GentR}$ phages**
649 A recombination substrate with a gentamicin resistance cassette flanked by homology
650 arms matching the DMS3m genome up and downstream of gp52 (450 bp and 260 bp,
651 respectively) was assembled into pHERD20T using Gibson assembly. This
652 recombination cassette was transformed into PA14 ∆CRISPR lysogenized with either
653 DMS3m$_{acrIE3}$ or DMS3m$_{acrIF1}$.These transformed lysogens were grown under gentamicin
654 selection for 16 h, then sub-cultured 1:100 into LB with gentamicin and 0.2 µg/mL
655 mitomycin C to induce the DMS3m$_{acr}$ prophage. Supernatants were harvested after 24
656 hours of induction, and used to infect PA14 ∆CRISPR for 24 h. These cells were then
657 plated on gentamicin plates to select for cells that had acquired a prophage bearing the
658 gentamicin resistance cassette, and gentamicin resistant lysogens were then re-induced
659 with 0.2 µg/mL mitomycin C to recover the recombinant phage.
660
661 **Construction of DMS3m$_{acr\ gp1\text{-}JBD30}$ (Hybrid$_{acr}$) phages**
662 DMS3m$_{acrIE3}$ and JBD30$_{acrIE3}$ were used to co-infect PA14 ∆CRISPR and the infected
663 cells were mixed with molten top agar and poured onto solid plates. After 24 hours of
664 growth at 30C, the phages were harvested by flooding the plate with SM buffer and
665 collecting and clarifying the supernatant. Phages were then used to infect PA14
666 ∆CRISPR expressing the DMS3 C repressor from pHERD30T, and the infections were
667 mixed with molten top agar and poured onto solid plates. After 24 hours of growth at 30
668 ºC, individual plaques with DMS3 morphology were picked, purified 3x by passage in
669 PA14 ∆CRISPR and screened as shown in Figure S4B.
670
671 **Phage (PFU) quantification**
672 Phage plaque forming units (PFU) were quantified by mixed 10µl of phage at a with 150
673 µl of an overnight culture of host bacteria. The infection mixture was incubate at 37 ºC
674 for 10 minutes to promote phage adsorption, then mixed with 3 mLs molten top agar and

675 spread on an LB agar plate supplemented with 10 mM $MgSO_4$. After 16 hours of growth
676 30 ºC, PFUs were quantified.
677
678 **Phage titering**
679 A bacterial lawn was generated by spreading 3 mLs of top agar seeded with 150 µl of
680 host bacteria on a LB agar plate supplemented with 10 mM $MgSO_4$. 3 µl of phage
681 serially diluted in SM buffer was then spotted onto the lawn, and incubated at 30 ºC for
682 16 hours.
683
684 **Measurement of anti-CRISPR binding kinetics by surface plasmon resonance**
685 Purified Csy complex was covalently immobilized by amine coupling to the surface of a
686 carboxymethyldextran-modified (CM5) sensor chip. Purified 6his-tagged AcrIF4 was
687 injected into the buffer flow in increasing concentrations (1.85 nM, 55.6 nM, 167 nM, 500
688 nM, 1.5 uM), and Csy complex-AcrIF4 binding events were recorded in real time.
689 Experiments were conducted at 37°C, in 20 mM HEPES pH 7.5, 100 mM KCl, 1mM
690 TCEP, 0.005% Tween. Data were fit with a model describing Langmuir binding (i.e. 1:1
691 binding between free analyte and immobilized ligand). Kinetic rate constants were
692 calculated using Biacore evaluation software (GE).
693
694 **Liquid culture phage infections**
695 Liquid culture phage infections and growth curves were performed by infecting 140 µl of
696 *P. aeruginosa* 1:100 diluted overnights cultured in LB supplemented with 10 mM MgSO4
697 and antibiotics and inducer in a 96 well costar plate with 10 µl of phage diluted in SM
698 buffer. These infections proceeded for 24 hours in a BioTek Synergy microplate reader
699 at 37 ºC with continuous shaking. After 24 hours, phage was extracted treating each
700 sample with chloroform followed by centrifugation at 21,000 x g for 2 minutes.
701
702 **Lysogen acquisition and induction**
703 Overnight cultures of PA14 were subcultured at 1:100 for ~3 hours (OD_{600nm} = 0.3) in LB
704 supplemented with 10 mM MgSO4. 1 mL of cells were then infected with 10 µl DMS3m$_{acr}$
705 $_{gp52::GentR}$ and incubated for 50 minutes at 37 ºC, shaking at 100 rpm. The sample was
706 then treated with a 10% volume of 10X gentamicin, spun down at 8,000xg, and
707 resuspended in 200 ul of LB with 50 µg/mL gentamicin. 100 ul of sample was then plated
708 (after further dilution, if required) on gentamicin selection plates and incubated at 37 ºC.
709 To analyze the lysogens, the resulting colonies were grown for 16 hours in LB + 10 mM
710 MgSO4 (no selection), the supernatants harvested, and serial dilutions spotted onto a
711 lawn of PA14 ∆CRISPR. Crude genomic DNA for PCR analysis was harvested from the
712 lysogens by boiling 10 µl of culture in 0.02% SDS for 10 minutes.
713
714 **Lysogen PCR**
715 PCR amplification of 2 µl of crude genomic DNA harvested from lysogens was used to
716 screen for the presence of *DMS3m-gp52* and *gentR* using MyTaq (Bioline) polymerase
717 with MyTaq GC buffer under standard conditions.
718

Figure 1

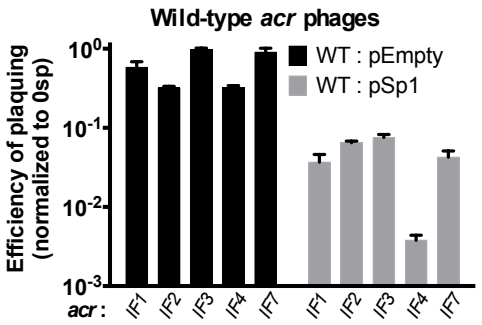
A
Wild-type acr phages
Efficiency of plaquing (normalized to 0sp)
WT : pEmpty
WT : pSp1
acr :
IF1
IF2
IF3
IF4
IF7

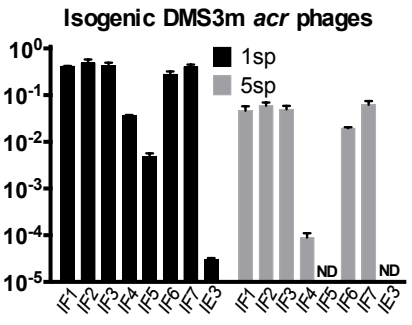
B
Isogenic DMS3m acr phages
1sp
5sp
ND
IF1
IF2
IF3
IF4
IF5
IF6
IF7
IE3

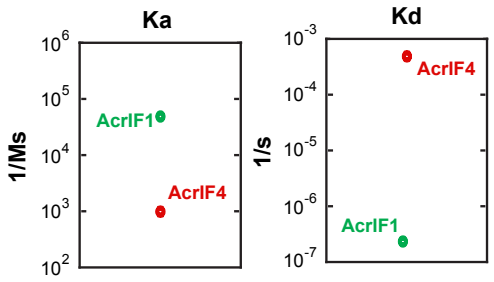
C
Ka
Kd
1/Ms
1/s
AcrIF1
AcrIF4

Figure 2

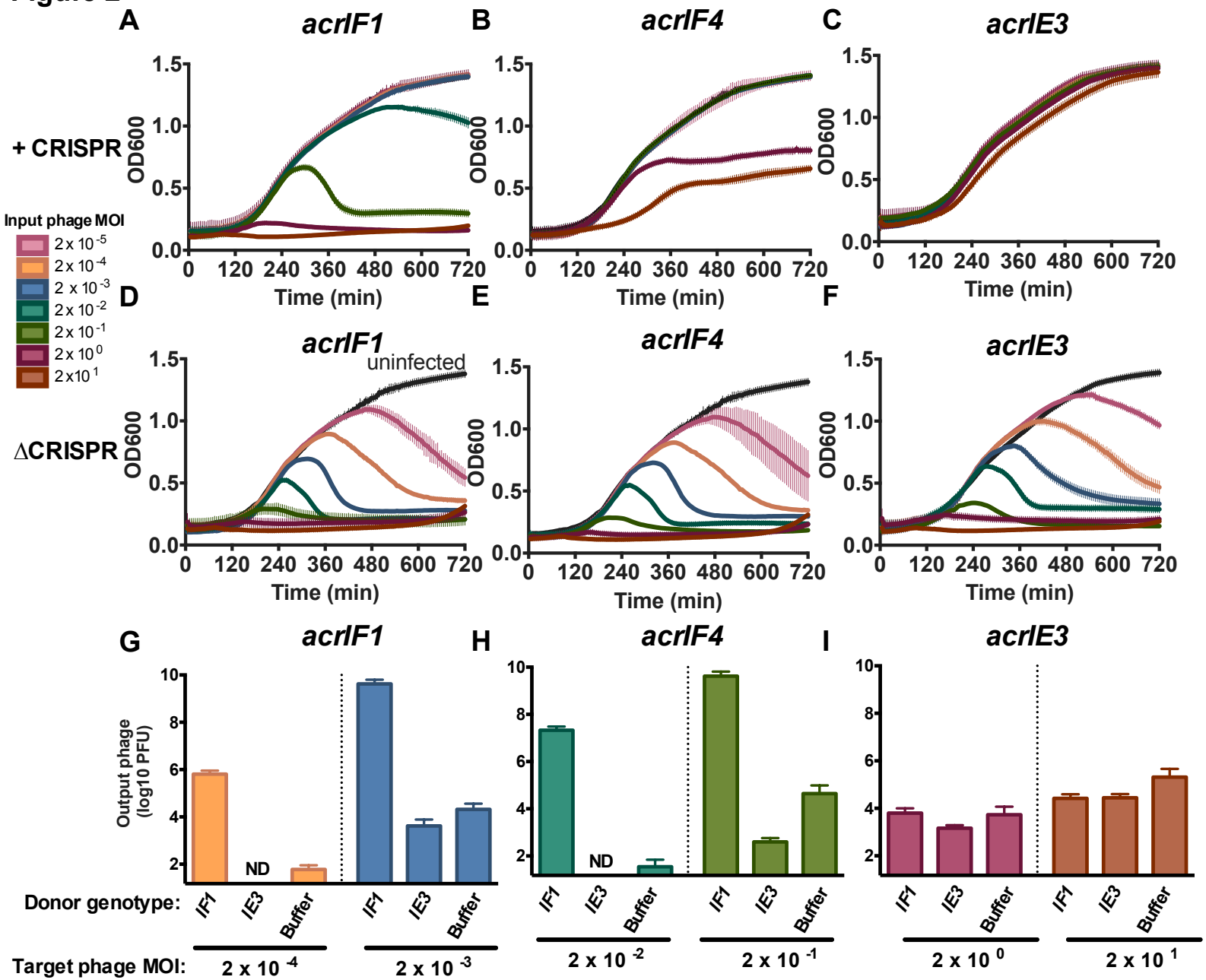
A
acrIF1
B
acrIF4
C
acrIE3
+ CRISPR
OD600
Time (min)
Input phage MOI
2 x 10 -5
2 x 10 -4
2 x 10 -3
2 x 10 -2
2 x 10 -1
2 x 10 0
2 x10 1
D
E
F
ΔCRISPR
uninfected
G
H
I
Output phage (log10 PFU)
ND
Donor genotype:
IF1
IE3
Buffer
Target phage MOI:
2 x 10 -4
2 x 10 -3
2 x 10 -2
2 x 10 -1
2 x 10 0
2 x 10 1

Figure 3

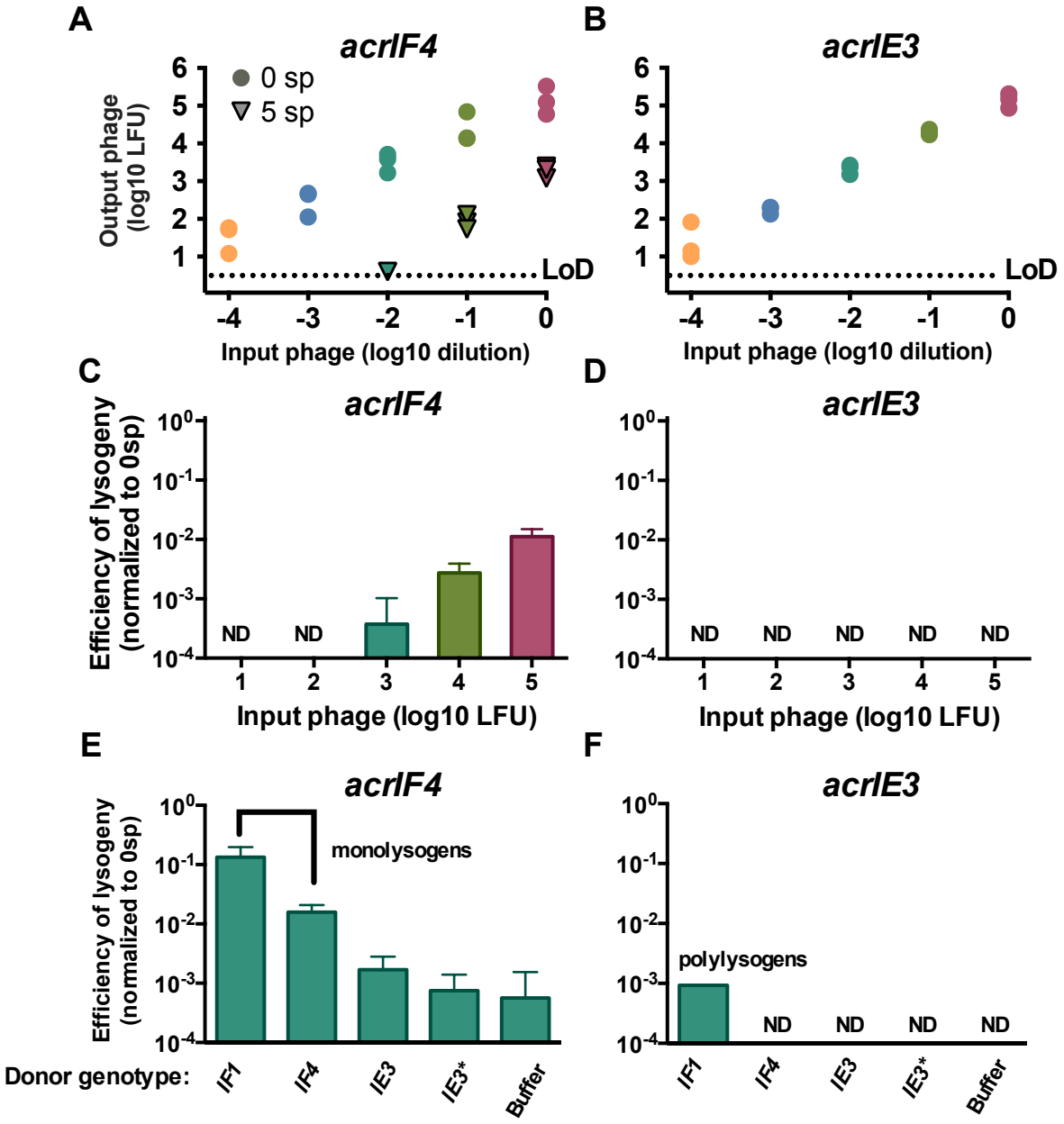
A
acrIF4
0 sp
5 sp
Output phage (log10 LFU)
LoD
Input phage (log10 dilution)
B
acrIE3
LoD
Input phage (log10 dilution)
C
acrIF4
Efficiency of lysogeny (normalized to 0sp)
ND
ND
Input phage (log10 LFU)
D
acrIE3
ND
ND
ND
ND
ND
Input phage (log10 LFU)
E
acrIF4
monolysogens
Efficiency of lysogeny (normalized to 0sp)
Donor genotype:
IF1
IF4
IE3
IE3*
Buffer
F
acrIE3
polylysogens
ND
ND
ND
ND
IF1
IF4
IE3
IE3*
Buffer

Figure 4

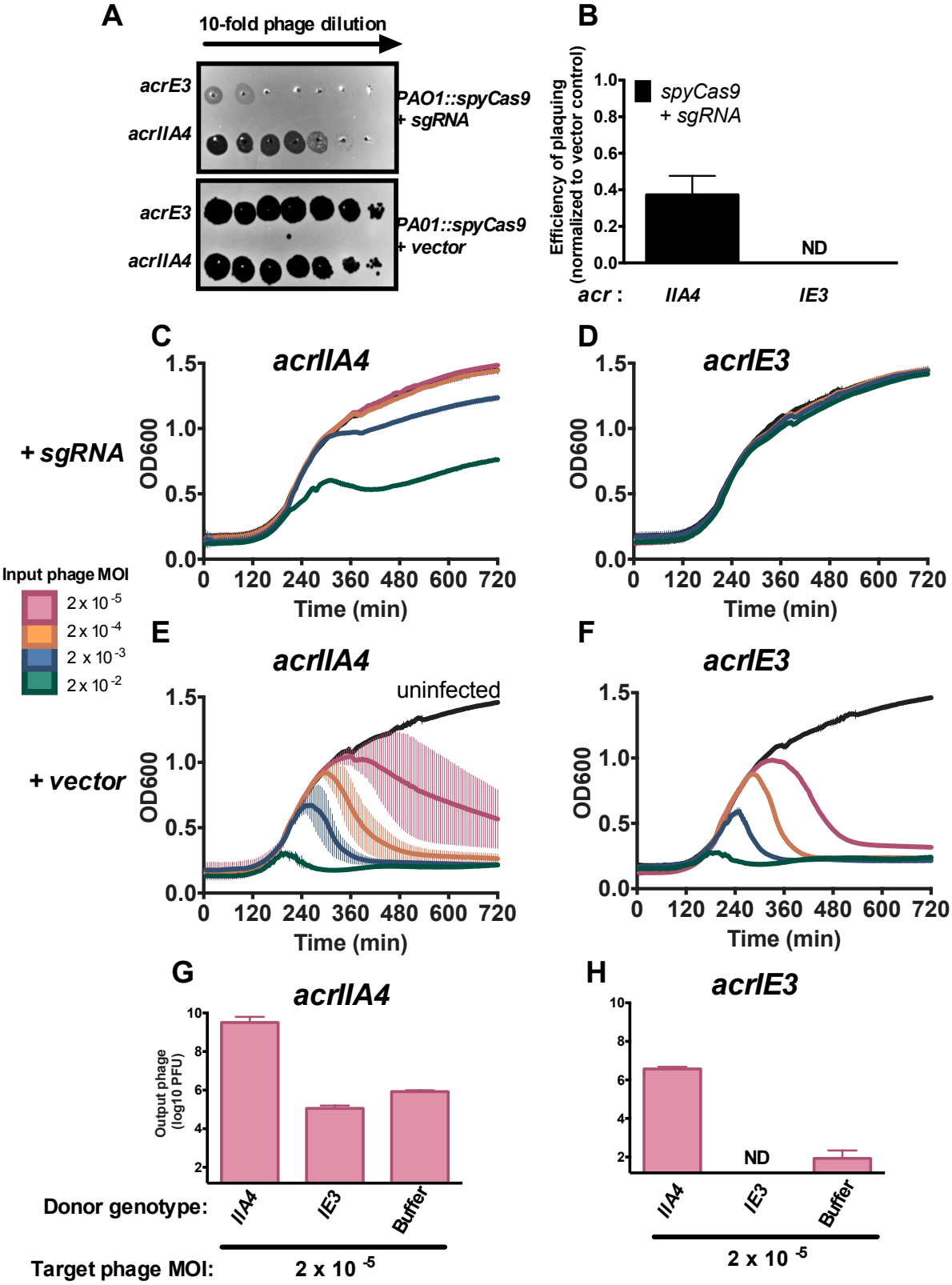
A
10-fold phage dilution
acrE3
acrIIA4
PAO1::spyCas9
+ sgRNA
acrE3
acrIIA4
PA01::spyCas9
+ vector
B
Efficiency of plaquing
(normalized to vector control)
spyCas9
+ sgRNA
ND
acr :
IIA4
IE3
C
acrIIA4
+ sgRNA
OD600
Time (min)
D
acrIE3
OD600
Time (min)
Input phage MOI
2 x 10 -5
2 x 10 -4
2 x 10 -3
2 x 10 -2
E
acrIIA4
uninfected
+ vector
OD600
Time (min)
F
acrIE3
OD600
Time (min)
G
acrIIA4
Output phage
(log10 PFU)
Donor genotype:
IIA4
IE3
Buffer
Target phage MOI:
2 x 10 -5
H
acrIE3
ND
IIA4
IE3
Buffer
2 x 10 -5

Figure 5

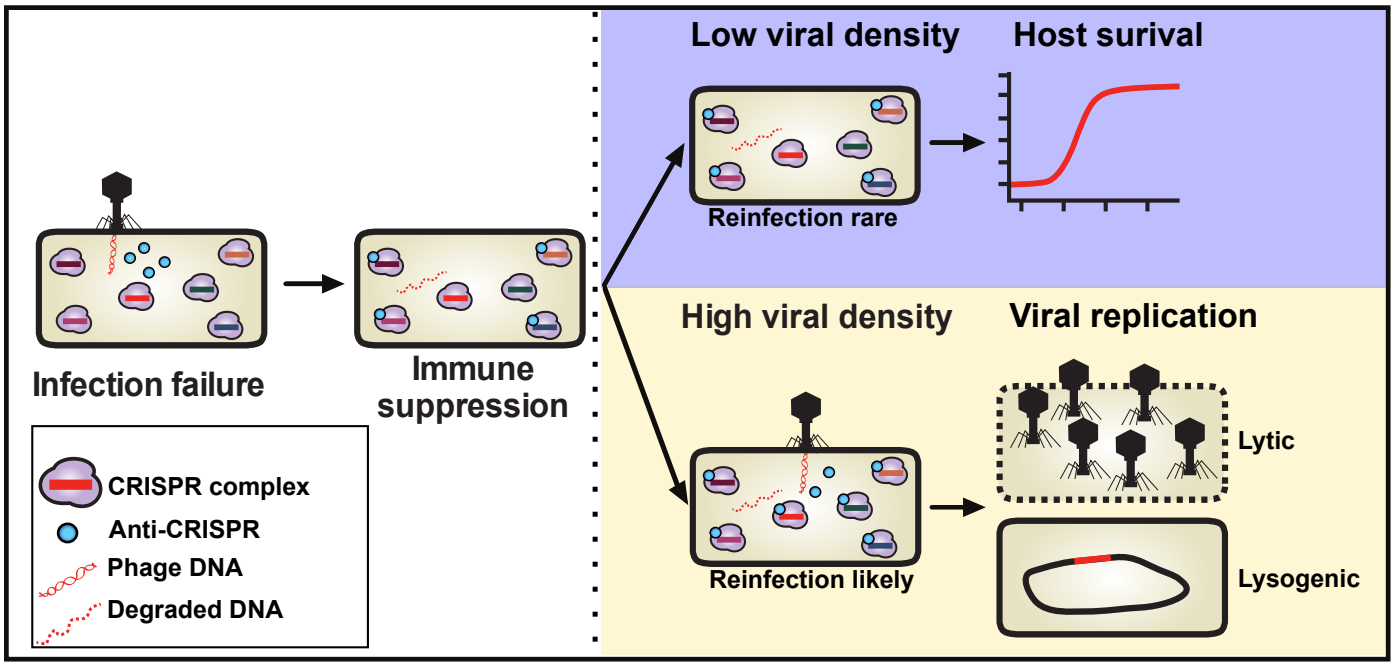
Low viral density
Host surival
Reinfection rare
Infection failure
Immune suppression
High viral density
Viral replication
Lytic
Reinfection likely
Lysogenic
CRISPR complex
Anti-CRISPR
Phage DNA
Degraded DNA

Supplementary Figure 1

A

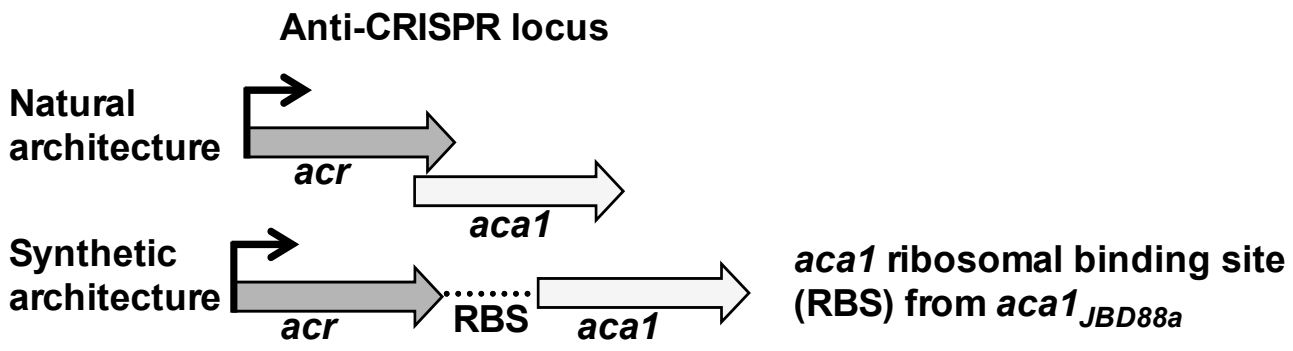

B

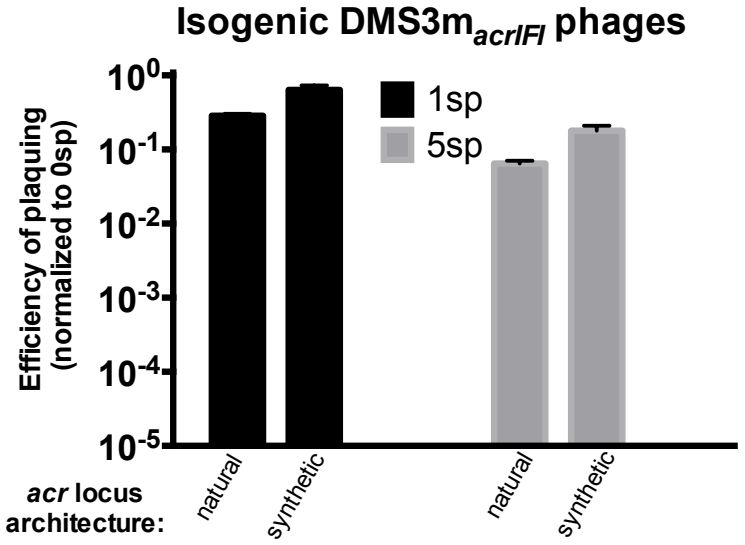

C **DMS3m$_{acr}$ phages**

Phage	DMS3m$_{acr}$ architecture	*acr* gene source	Acr Accession
DMS3m$_{acrIE3}$ (parent phage, no manipulation)	natural	DMS3m (gp30)	WP_003723290.1
DMS3m$_{acrIF1}$	natural	JBD30 (gp35)	YP_007392342.1
DMS3m$_{acrIF2}$	natural	MP29 (gp29)	YP_002332454.1
DMS3m$_{acrIF3}$	natural	JBD88a (gp33)	YP_007392440.1
DMS3m$_{acrIF4}$	natural	JBD26 (gp37)	WP_016068584.1
DMS3m$_{acrIF5}$	synthetic	JBD5 (gp36)	YP_007392740.1
DMS3m$_{acrIF6}$	synthetic	*Pseudomonas aeruginosa* strain PSE05 (prophage)	WP_043884810.1
DMS3m$_{acrIF7}$	natural	LPB1 (gp29)	YP_009146150.1
DMS3m$_{acrIIA4}$	synthetic	*Listeria monocytogenes* J0161 (prophage)	WP_003723290.1

Supplementary Figure 2

A

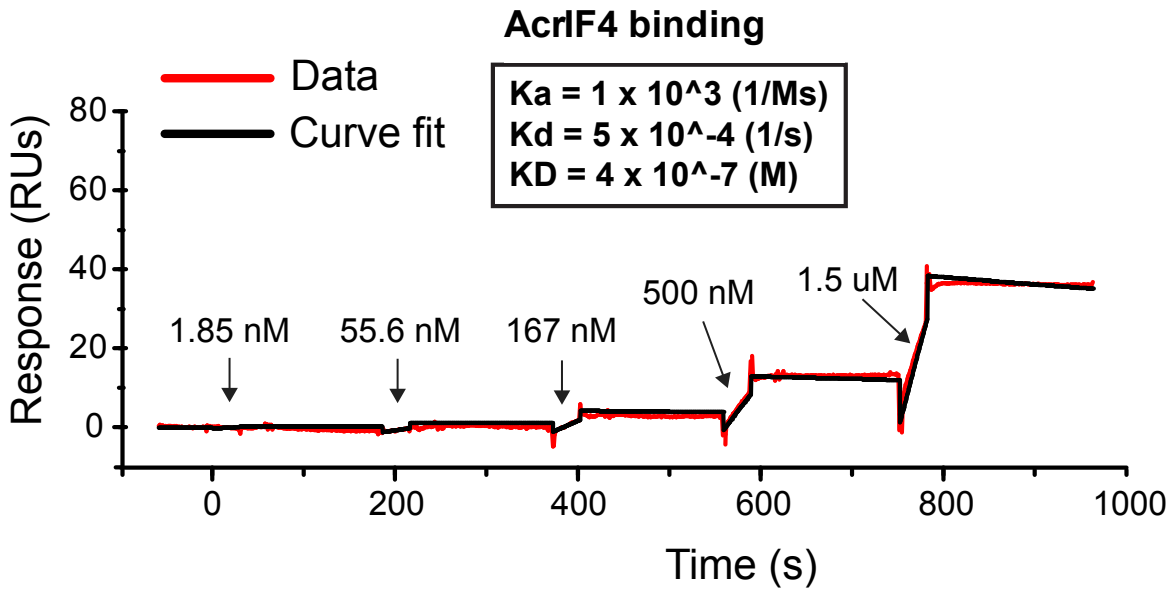

Supplementary Figure 3

A

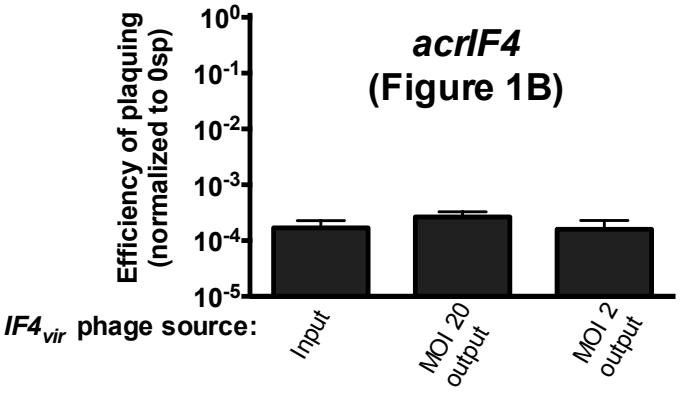

Supplementary Figure 4

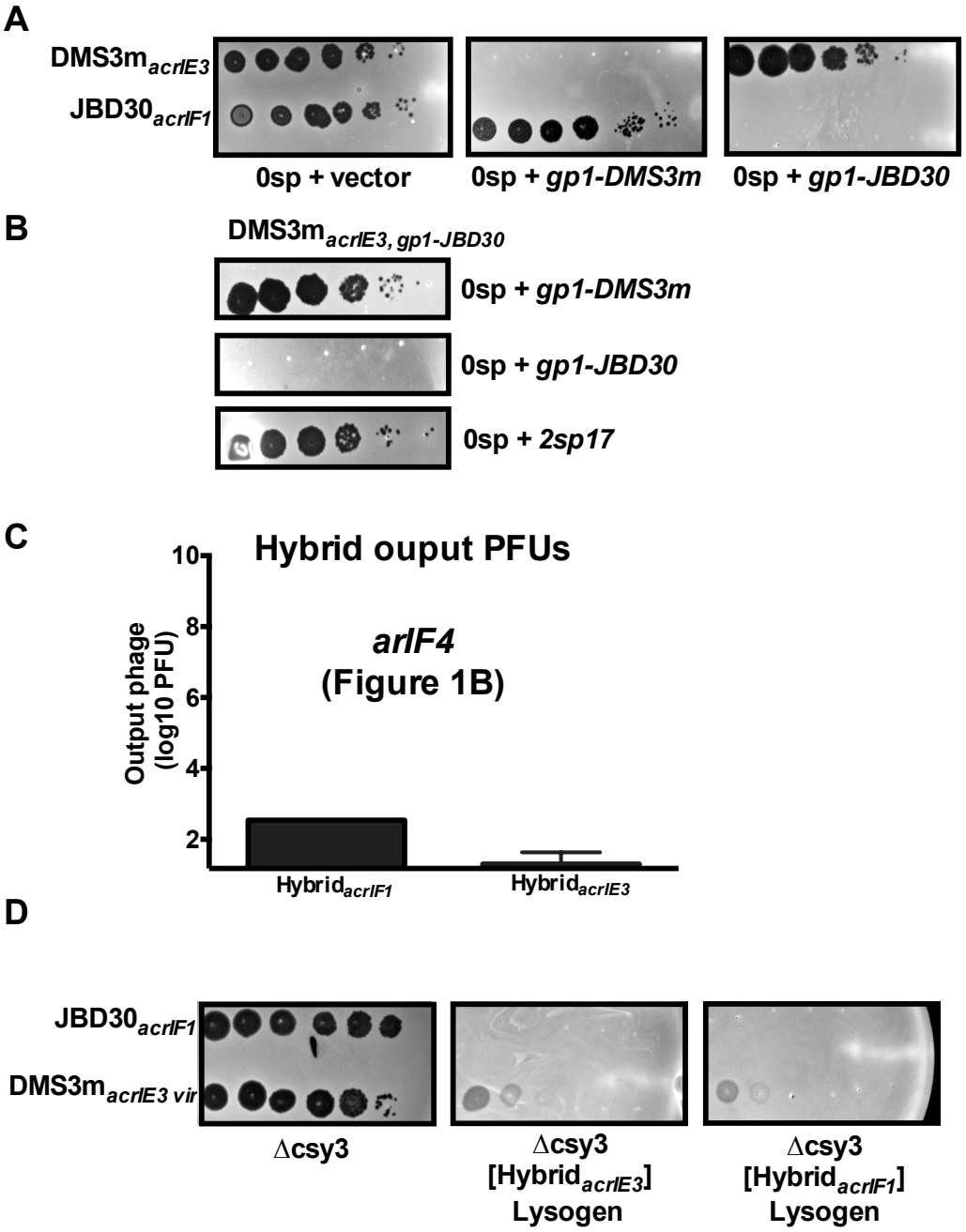

Supplementary Figure 5

A

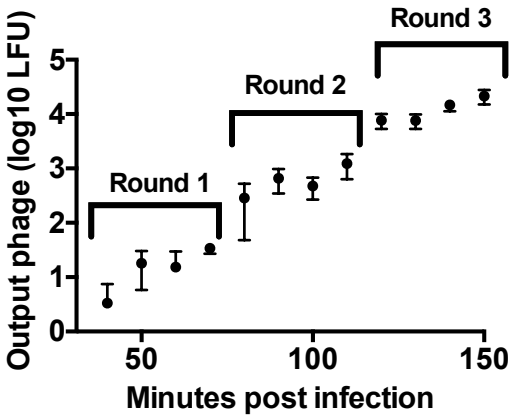

Supplementary Figure 6

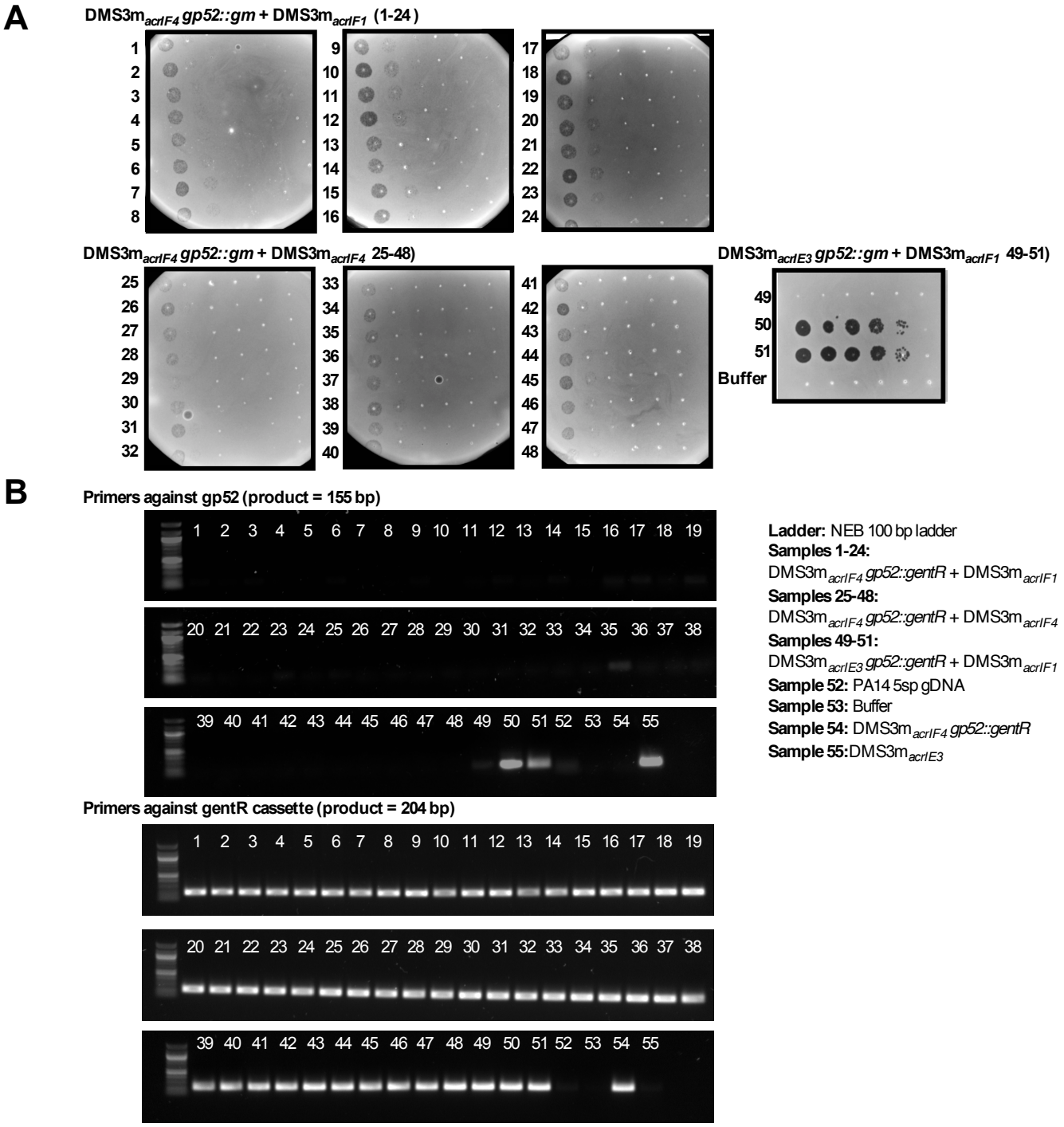

Plasmid table:

Plasmid	Backbone	Purpose
CR2sp17-OE	pHERD 30T	crRNA overexpression
CR2sp20-OE	pHERD 30T	crRNA overexpression
acrF2-flip	pHERD 30T	generating DMS3m$_{acrIF2}$
acrF3-flip	pHERD 30T	generating DMS3m$_{acrIF3}$
acrF4-flip	pHERD 30T	generating DMS3m$_{acrIF4}$
acrF5-synthetic-flip	pHERD 30T	generating DMS3m$_{acrIF5}$
acrF6-synthetic-flip	pHERD 30T	generating DMS3m$_{acrIF6}$
acrF7-flip	pHERD 30T	generating DMS3m$_{acrIF7}$
acrIIA4-synthetic-flip	pHERD 30T	generating DMS3m$_{acrIIA4}$
gp52::gentR-flip	pHERD 20T	generating DMS3m$_{acr\ gp52::gentR}$
gp1-JBD30	pHERD 20T and 30T	C repressor (JBD30) overexpression
gp1-DMS3	pHERD 20T and 30T	C repressor (DMS3) overexpression
sgRNA-DMS3	pMMBHE	DMS3m targeting with SpyCas9
SpyCas9- pLac	pUC18T-mini-Tn7T-Gm	Insertion of SpyCas9 into the PAO1 tn7 site